Supporting Information

Degradation of tetrabromobisphenol A by sulfidated nanoscale zerovalent iron in a dynamic two-step anoxic/oxic process

Jun Wu[†,‡,⊥,#], *Jian Zhao*[§,#], *Jun Hou*[∥,⊥], *Raymond Jianxiong Zeng*[†,‡,*], *Baoshan Xing*[⊥,*]

[†]Centre of Wastewater Resource Recovery, College of Resources and Environment, Fujian Agriculture and Forestry University, Fuzhou, Fujian 350002, China

[‡]CAS Key Laboratory for Urban Pollutant Conversion, Department of Applied Chemistry, University of Science & Technology of China, Hefei 230026, China

[§]Institute of Coastal Environmental Pollution Control, and Key Laboratory of Marine Environment and Ecology, Ministry of Education, Ocean University of China, Qingdao 266100, China

[∥]Key Laboratory of Integrated Regulation and Resources Development on Shallow Lakes of Ministry of Education, College of Environment, Hohai University, Nanjing, 210098, China

[⊥] Stockbridge School of Agriculture, University of Massachusetts, Amherst, Massachusetts 01003, United States

[#]These two authors contributed equally to this work.

Name of the journal: ***Environmental Science & Technology***
Date of the document prepared: May 17, 2019

Chemicals, preparation of nZVI, FeS, tri-BBPA, di-BBPA, and mono-BBPA, extraction and characterization of HA, transformation kinetics of TBBPA, chemical analysis, and characterization.

Number of pages = 35
Number of tables = 6
Number of figures = 13

Chemicals

$FeSO_4 \cdot 7H_2O$, sodium borohydride, and TBBPA (97%) were purchased from Alfa Aesar. H_2O_2 and BPA (99%) were obtained from Sigma–Aldrich (MO, USA). Ethanol, H_2O_2, sodium benzoate, 2, 2'-bipyridine (BPY), sodium ethylene diamine tetracetate (Na_2EDTA), p-hydroxybenzoic acid (*p*-HBA) 1,10-phenanthroline, acetonitrile, carbon disulfide (CS_2), HCl, bromine, sodium sulfate, sodium thiosulfate, phenol were purchased from Fisher Scientific (NJ, USA). $Na_2S \cdot 9H_2O$ was obtained from MP Biomedicals (CA, USA). NaOH was purchased Acros Organics (NJ, USA). Tri-BBPA, di-BBPA, mono-BBPA were synthesized according to the method reported by Eriksson et al.[1] Detailed description about the preparation is shown as below (SI).

Preparation of nZVI and FeS

20.00g $FeSO_4 \cdot 7H_2O$ was dissolved into a 30% (volume) methanol/DI water solution to obtain a 0.07 M $FeSO_4 \cdot 7H_2O$ solution, and 5 M NaOH aqueous solution was added dropwise to the dissolved iron solution. Subsequently, 50 mL of 0.019 M $NaBH_4$ was added drop-wise to the iron solution using a syringe pump while stirring. After adding all the $NaBH_4$ solution, the obtained solution was stirred for another one hour. The resulting suspension was washed three times with methanol and dried under nitrogen and stored in sealed vials in an anaerobic glove box containing high purity N_2/H_2 (95%/5%).

The FeS nanoparticle suspension was prepared through the approach developed in a prior work.[2] Briefly, a 0.043 M $FeCl_2$ solution (31.7 mL) was added to 52.4 mL DI water purged with N_2 for 30 min. Subsequently, a stoichiometric amount of 0.085 M Na_2S solution (15.9 mL) was added dropwise to the solution in an anaerobic glove box containing 5% hydrogen and 95% nitrogen. Addition was done using a syringe, and the solution was mixed through vortexing. The resultant nanoparticle suspension consisted of 1.2 g/L FeS. To ensure complete reaction and full growth of the nanoparticles, the suspension was sealed and aged for 24 h before use.

Hydrogen Evolution Assay

H_2 evolution of S-nZVI and nZVI was measured in DI water at pH = 6.0±0.2 over time. 100 mL of S-nZVI or nZVI suspensions (1.2 g/L) were placed in 150-mL glass vials sealed by butyl rubber, respectively. The headspace in the vial was sampled with a gas-tight syringe (SGE Analytical Science, Australia) to determine H_2 by a gas chromatograph (Shimadzu GC-14B, Japan). In order to quantify H_2, the vials were sparged with high purity N_2 to remove the generated H_2 out from vials after each sampling.

The production of H_2O_2 and •OH during oxic stage

The concentrations of H_2O_2 and •OH were recorded with the same procedures during oxic stage. Cumulative •OH was measured by employing the transformation of benzoate to p-hydroxybenzoic acid (*p*-HBA) as a probe reaction.[3] The concentration of *p*-HBA was measured by a Shimadzu Prominence high performance liquid chromatography (HPLC) system (Shimadzu, Japan) with the detection wavelength at 255 nm. The mobile phase was a mixture of 0.1% trifluoroacetic acid aqueous solution and acetonitrile (65:35, v/v) at a flow rate of 1 mL min^{-1}. A conversion factor of 5.87 was used to estimate the cumulative •OH concentrations.[4] H_2O_2 was analyzed by a modified DPD method, and 2, 2′-bipyridine (BPY) and sodium ethylene diamine tetracetate (Na_2EDTA) were added to complex Fe(II) and Fe(III), respectively, to minimize their interference.[5] For comparison, the production of H_2O_2 and •OH with addition of 1 M ethanol under anoxic conditions were carried out.

Preparation of tri-BBPA, di-BBPA, and mono-BBPA

BPA (1.0 g, 4.4 mmol) was dissolved in acetic acid (400 ml) and bromine (0.7 ml, 13 mmol) was added to the solution. The reaction mixture was stirred at room temperature for 1.5 h. Water (200 ml) was added, the mixture was neutralized with sodium hydrogen carbonate and then extracted with dichloromethane. The organic phase was dried over sodium sulphate. The solvent was evaporated and the product was purified on an open silica gel column (Merck, 0.040–0.063 mm) with dichloromethane as the mobile phase. The product was recrystallised in hexane. The yield of tri-BBPA was 1.03 g (2.2 mmol, 51%). HPLC and GC–MS analysis demonstrated that the final tri-BBPA purity was >97%. Similarly, di-BBPA and mono-BBPA were prepared with same method described above according to the different ratio of BPA/bromine. That is say, 0.467 mL and 0.233 mL of bromine were added BPA (1.0 g, 4.4 mmol) acetic acid solution to prepare di-BBPA and mono-BBPA, respectively.

Extraction and characterization of HA

HA extraction involved mixing peat (air-dried and passed through a 2-mm sieve) with 0.1 mol/L NaOH at a solid to solution ratio of 10:1 (v:w) in a 1000-mL bottle. The air in the bottle was replaced with N_2 gas, and the mixture was shaken for 24 h at room temperature. After being mixed, the suspension was centrifuged at 3500g for 30 min, and the supernatant was collected for acidification (pH 1.5 with 1.0 mol/L HCl) to obtain HA. Precipitated HA in acidified supernatant was separated and collected by centrifugation at 3500g for 30 min. After that, HA was de-ashed three times using 0.1 M HCl and 0.3 M HF mixtures at a ratio (g/mL) of 1:20, rinsed with deionized water, freeze-dried, gently ground to pass through a 100-μm sieve, and stored for subsequent use.

The C, H, and N contents of the HA were determined using a Perkin-Elmer 2400 CHN Elemental Analyzer (Shelton, USA). Oxygen content was calculated by the mass difference. Ash content was measured by heating the samples at 800 °C for 4 h. A Fourier transform infrared (FTIR) spectrometer (Varian 640-IR, Varian, USA) was used to characterize the functional groups of HA. The results are shown in Table S1 and Figure S1. Bands at 3360, 2925, 2855, 1655, 1545, and 1060 cm^{-1} were assigned to the stretching of −OH, $-CH_3$, $-CH_2$, −C=O, aromatic −C=C, and −C–O groups, respectively.

Transformation kinetics of TBBPA

The rate models for quantifying transformation kinetics of TBBPA in the S-nZVI systems were proposed, in which each step of the sequential reactions followed a typical pseudo-first order rate as shown below (eq. (1)):

$$\text{TBBPA} \xrightarrow{k_1} \text{tri-BBPA} \xrightarrow{k_2} \text{di-BBPA} \xrightarrow{k_3} \text{mono-BBPA} \xrightarrow{k_4} \text{BPA} \quad \text{(S1)}$$

According to the law of mass conservation and stoichiometry of the reaction, the differential equations of the rate expressions involving the reactant, intermediates, and final product are shown below:

$$\frac{d[\text{TBBPA}]}{dt} = -k_1[\text{TBBPA}] \quad \text{(S2)}$$

$$\frac{d[\text{tri-BBPA}]}{dt} = k_1[\text{TBBPA}] - k_2[\text{tri-BBPA}] \quad \text{(S3)}$$

$$\frac{d[\text{di-BBPA}]}{dt} = k_2[\text{tri-BBPA}] - k_3[\text{di-BBPA}] \quad \text{(S4)}$$

$$\frac{d[\text{mono-BBPA}]}{dt} = k_3[\text{di-BBPA}] - k_4[\text{mono-BBPA}] \quad \text{(S5)}$$

$$\frac{d[\text{BPA}]}{dt} = k_4[\text{mono-BBPA}] \quad \text{(S6)}$$

$$C_0 = [\text{TBBPA}] + [\text{tri-BBPA}] + [\text{di-BBPA}] + [\text{mono-BBPA}] + [\text{BPA}] \quad \text{(S7)}$$

where k_1, k_2, k_3 and k_4 (h^{-1}) are the rate constants of the reaction at corresponding steps; [TBBPA], [tri-BBPA], [di-BBPA], [mono-BBPA], and [BPA] are the concentrations of TBBPA, tri-BBPA, di-BBPA, mono-BBPA, and BPA (μM) at time t. At time 0, the initial concentrations of tri-BBPA, di-BBPA, mono-BBPA and BPA all were equal to 0, 0, 0, and 0 μM, respectively.

Integration of eq. (2) to eq. (7) step by step yielded:

$$[\text{TBBPA}] = [\text{TBBPA}]_0 e^{-k_1 t} \tag{S8}$$

$$[\text{tri-BBPA}] = \frac{k_1[\text{TBBPA}]_0}{k_2 - k_1}\left(e^{-k_1 t} - e^{-k_2 t}\right) \tag{S9}$$

$$[\text{di-BBPA}] = k_1 k_2 [\text{TBBPA}]_0 \left[\frac{e^{-k_1 t}}{(k_2 - k_1)(k_3 - k_1)} + \frac{e^{-k_2 t}}{(k_1 - k_2)(k_3 - k_2)} + \frac{e^{-k_3 t}}{(k_1 - k_3)(k_2 - k_3)}\right] \tag{S10}$$

$$[\text{mono-BBPA}] = k_1 k_2 k_3 [\text{TBBPA}]_0 \left[\frac{e^{-k_1 t}}{(k_2 - k_1)(k_3 - k_1)(k_4 - k_1)} + \frac{e^{-k_2 t}}{(k_1 - k_2)(k_3 - k_2)(k_4 - k_2)} + \frac{e^{-k_3 t}}{(k_1 - k_3)(k_2 - k_3)(k_4 - k_3)} + \frac{e^{-k_4 t}}{(k_1 - k_4)(k_2 - k_4)(k_3 - k_4)}\right] \tag{S11}$$

$$[\text{BPA}] = [\text{TBBPA}]_0 \left[1 - \frac{k_1 k_2 k_3}{(k_2 - k_1)(k_3 - k_1)(k_4 - k_1)} e^{-k_1 t} - \frac{k_1 k_2 k_3}{(k_1 - k_2)(k_3 - k_2)(k_4 - k_2)} e^{-k_2 t} - \frac{k_1 k_2 k_3}{(k_1 - k_3)(k_2 - k_3)(k_4 - k_3)} e^{-k_3 t} - \frac{k_1 k_2 k_3}{(k_1 - k_4)(k_2 - k_4)(k_3 - k_4)} e^{-k_4 t}\right] \tag{S12}$$

The values of rate constants (k_1, k_2, k_3, k_4) can be determined experimentally by plotting [TBBPA], [tri-BBPA], [di-BBPA] and [mono-BBPA] versus t.

Chemical analysis

The concentrations of TBBPA and its transformation products (i.e., tri-BBPA , di-BBPA , mono-BBPA and BPA) were determined by Shimadzu Prominence HPLC system (Shimadzu, Kyoto, Japan) with a reverse-phase C18 column (ZORBAX Eclipse Plus, 4.6 × 150 mm, 5.0 μm, Agilent, USA). The mobile phase was a mixture of methanol/water (v/v, 8/2) and the flow rate was 1.0 mL min^{-1}. The linear standard curves of TBBPA and its transformation products were obtained with the range from 0.9 to 2.2 μM, and the linear regression analysis of standard curves of TBBPA and its products showed good linearity (R^2 > 0.998). Identification of the transformation products of TBBPA were performed on an Agilent 1200 liquid chromatography coupled to an Agilent 6410 electrospray triple quadrupole mass spectrometer (LC-MS). The LC-MS analytical procedures including column, mobile phases, flow rates were identical to those of HPLC analysis described above.

The intermediate products of BPA degradation were determined using an Agilent 7890B gas chromatography-mass spectrometer (GC-MS) (Agilent, USA) equipped with an Agilent 5977B single quadrupole mass spectrometric detector. Mass spectra were acquired in electron ionization mode using a DB-5 fused-silica capillary column (30 m × 320 μm i.d × 0.25 mm film thickness). Prior to GC-MS analysis, the samples were extracted with dichloromethane for three times. The extracted solution was dehydrated using anhydrous sodium sulfate. The initial temperature of the column oven was 60 °C and following 5 min hold at this temperature, and then increased up to 300 °C with a heating rate of 10 °C min^{-1}. Helium gas was used as the carrier gas at a flow

rate of 1 mL min^{-1}.

Fe(0) content was determined from the H_2 content after acidification by 1M HCl. Fe(0) was dissolved to Fe(II) and total Fe (II) was detected by spectrophotometry using 1,10-phenanthroline and the method was described in detail in our previous study,[6] thus the Fe(II) in S-nZVI was calculated by deducting the F(0) from total Fe(II). Total iron was measured using an inductively coupled plasma mass spectrometry (ICP-MS) (Agilent 7500ce, USA), thus ferric ions (Fe(III)) was calculated by deducting total Fe(II) from total iron. The dissolved bromide ion, sulfate, thiosulfate were determined using ion chromatography (DIONEX ICS-1100, USA) equipped with an AS19 column and an electrical conductivity detector.

Elemental sulfur (S_8) was measured by a HPLC method that was developed in a prior study.[7] Briefly, at the specified intervals, 1 mL aliquots of slurries (mixtures of solution and solid) were also withdrawn from the reaction batches to quantify the production of S_8. Two milliliters of carbon disulfide (CS_2) were added to the slurries and shaken for 5 min inside the anaerobic chamber. Due to its high hydrophobicity, elemental sulfur was partitioned into the non-aqueous CS_2 phase. An aliquot of the organic phase was carefully taken and analyzed for elemental sulfur by a HPLC.

Characterization methods

Transmission electron microscopy (TEM) and elemental mapping analysis were conducted on a JEOL-2010 JSM microscope at an acceleration voltage of 200 kV. High resolution TEM (HRTEM) analysis was carried out with a JEOL JEM-ARF200F. Powder X-ray diffraction (XRD) patterns were recorded at a scanning rate of 0.02°/s in the 2θ range of 10°–60° on a Philips X'Pert ProSuper X-ray diffractometer using graphite-monochromatized Cu Kα radiation (λ = 1.54178 Å). MDI Jade 6.0 software was used to identify the mineral phases. X-ray photoelectron spectroscopy (XPS) was performed with a Thermo Escalab 250 (Thermo VG Scientific, West Sussex, UK) using a monochromatic Al Kα source (1486.6 eV). The intensity of each XPS peak was recorded in counts per second. XPS PEAK v4.0 was used to analyze and fit algorithm with a Gaussian–Lorentzian sum function. Nitrogen gas sorption data were gathered from a Micromeritics Tristar II 3020M (Micromeritics Instrument Co., Norcross, GA, USA) automated gas adsorption analyzer, to calculate the Barrett–Emmett–Teller (BET) surface area. All S-nZVI samples were powdered, vacuum freeze-dried, and then stored in an anaerobic glove box before characterization.

Characterization of S-nZVI

Fresh nZVI particles with particle size of ~30 nm show chain like aggregates (Figure S2a). After sulfidation, the S-nZVI displayed a slightly different morphology, having smaller particles (~20 nm) with more aggregated clusters (Figure S2b). This was consistent with a previous report using the same synthesis method.[8] The XRD pattern of the as-prepared S-nZVI showed intense peaks at 2θ = 17.6°, 30.1°, 39.0°, 50.3°, and 53.0°, which respectively corresponded to the (001), (101), (111), (112), and (201) planes of mackinawite (FeS) (JCPDS no. 89-2738), while the peak of Fe(0) at 2θ = 44.9 ° was also observed (Figure S3), suggesting the highly ordered crystallinity of S-nZVI. However, previous studies showed poorly ordered crystallinity of S-nZVI,[9, 10] which may be ascribed to the lower S/Fe molar ratio (0.14) and less aging time (15 min) than that in our study. The $2p_{3/2}$ XPS spectra of Fe and S in S-nZVI were fitted (Figure S4, Table S2). Fe was mainly in the form of Fe(II)–S species (73.3%; signals centered at 707.3), and little of it was in the form of Fe(II)–O and Fe(III)–S species before reaction (Figure S4a, Table S2). Fe(0) was not observed in XPS spectra, indicating that aqueous sulfide (as S^{2-} or HS^-) is a corrosive chemical and its attacking on iron resulted in deposition of a layer of FeS on the surface of nZVI.[8] XPS results for the S species suggest that S(−II), S_2(-II), and S_n(−II) comprised approximately 91.9% of the S (Figure S4b, Table S2). The rest trace of S species was S_8, which may be formed by the oxidation of oxygen during the test.[11]

Effect of HA

Degradation of both TBBPA and BPA was slightly inhibited by HA (Figures S12c-S12d), which was in agreement with the calculated rate constants of TBBPA and BPA, respectively (Table S6). For TBBPA, competitive adsorption of HA with TBBPA decreased the degradation of TBBPA by S-nZVI. For BPA, on the one hand, the formation of soluble Fe-humate complexes appeared to result in less Fe(II) being available for •OH production, because HA is known as a metal-complexing agent.[12] The total amount of dissolved Fe(II) steadily increased to 1.8 mM in the presence of HA (Figure S13). On the other hand, organic acids, such as HA could scavenge •OH, thus screening the oxidation of BPA caused by •OH.[13] It should be noted that the inhibition by HA was lower than that observed in previous studies,[14, 15] suggesting that this dynamic two-step anoxic/oxic process could potentially be applied in wastewater treatments.

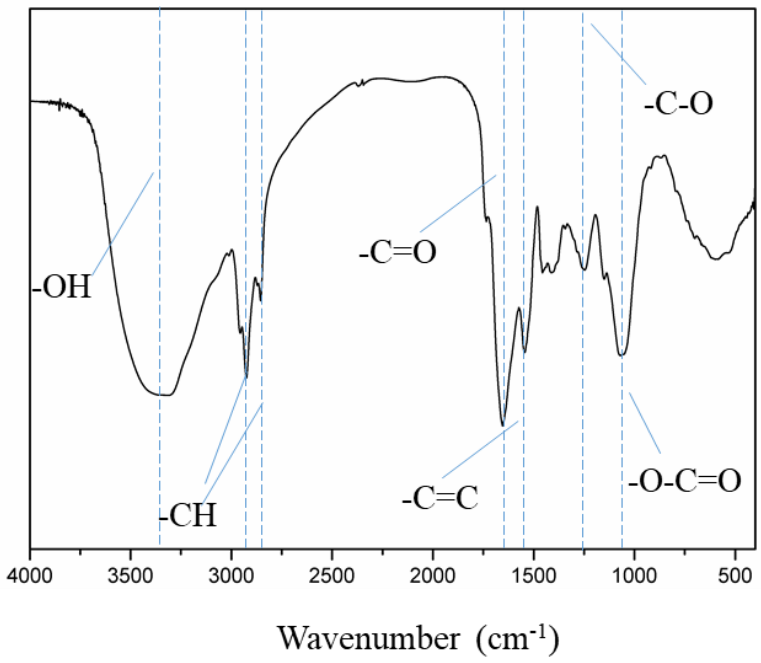

Figure S1. FTIR spectrum of HA.

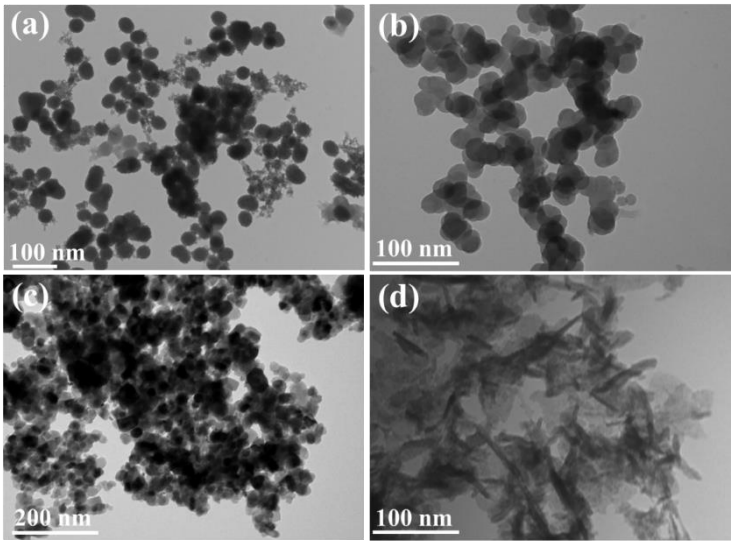

Figure S2. TEM images of (a) nZVI (b) pristine S-nZVI (c) S-nZVI after anoxic treatment and (d) S-nZVI after oxic treatment. S/Fe mole ratio = 0.3.

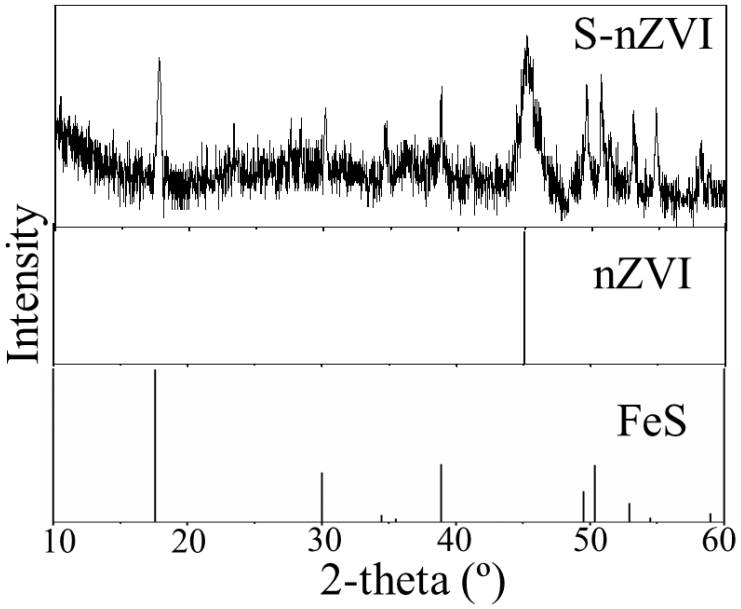

Figure S3. XRD patterns of the as-synthesized S-nZVI.

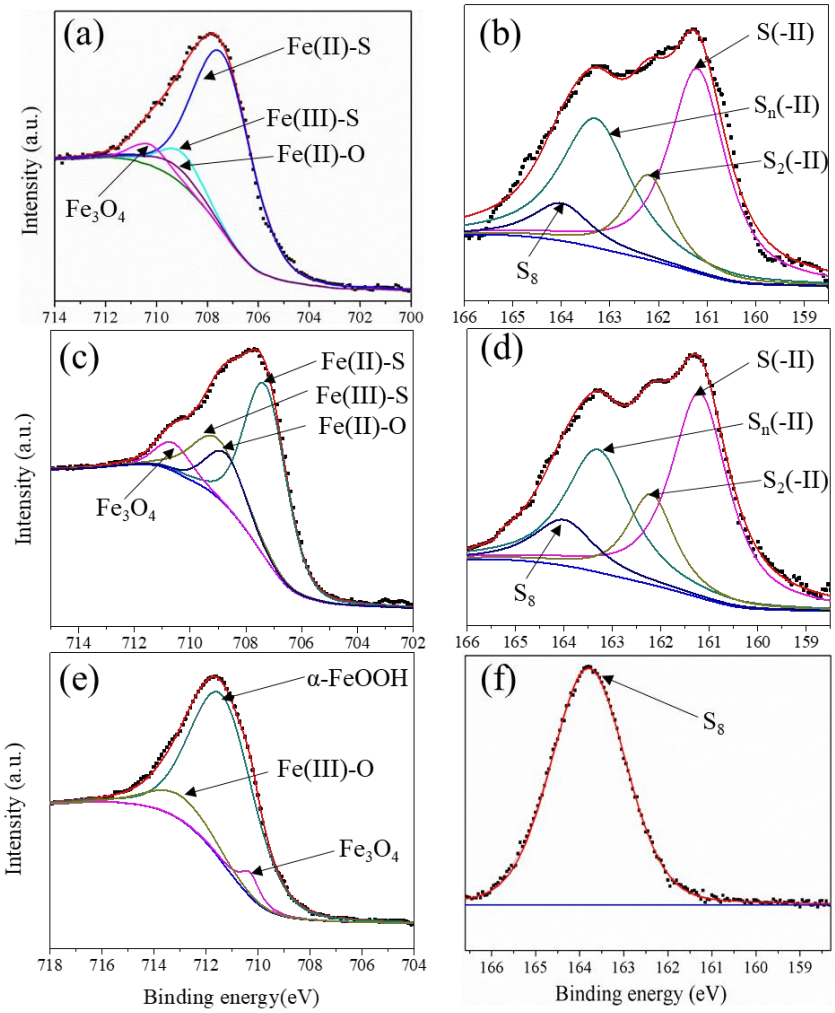

Figure S4. Fe and S XPS spectra: (a) Fe $2p_{3/2}$ (b) S $2p_{3/2}$ XPS spectrum of pristine S-nZVI. (c) Fe $2p_{3/2}$ (d) S $2p_{3/2}$ XPS spectrum of S-nZVI after anoxic treatment. (e) Fe $2p_{3/2}$ (f) S $2p_{3/2}$ XPS spectrum of S-nZVI after oxic treatment.

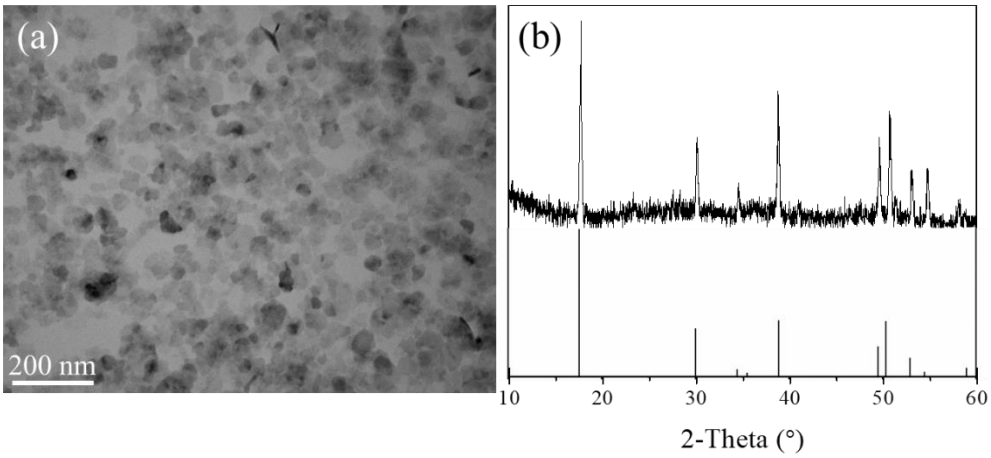

Figure S5. Characterization of the as-prepared FeS. (a) TEM image; (b) XRD pattern.

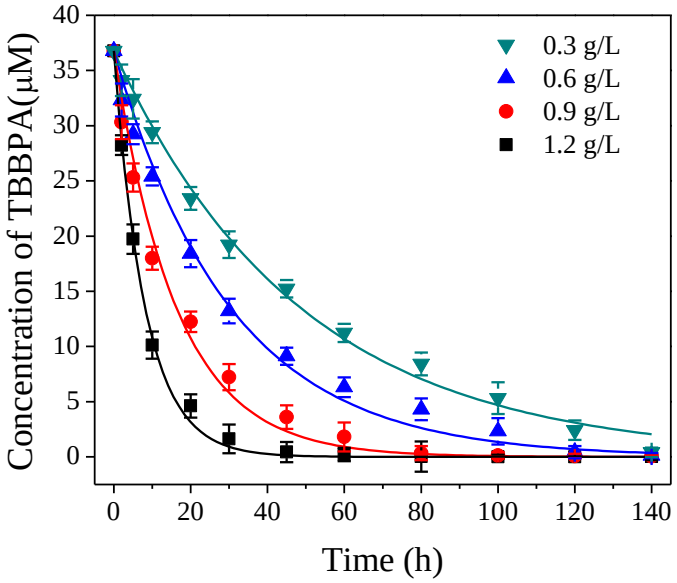

Figure S6. TBBPA degradation under different S-nZVI dosages under anoxic conditions. Initial pH = 6.0±0.2, S/Fe molar ratio = 0.3.

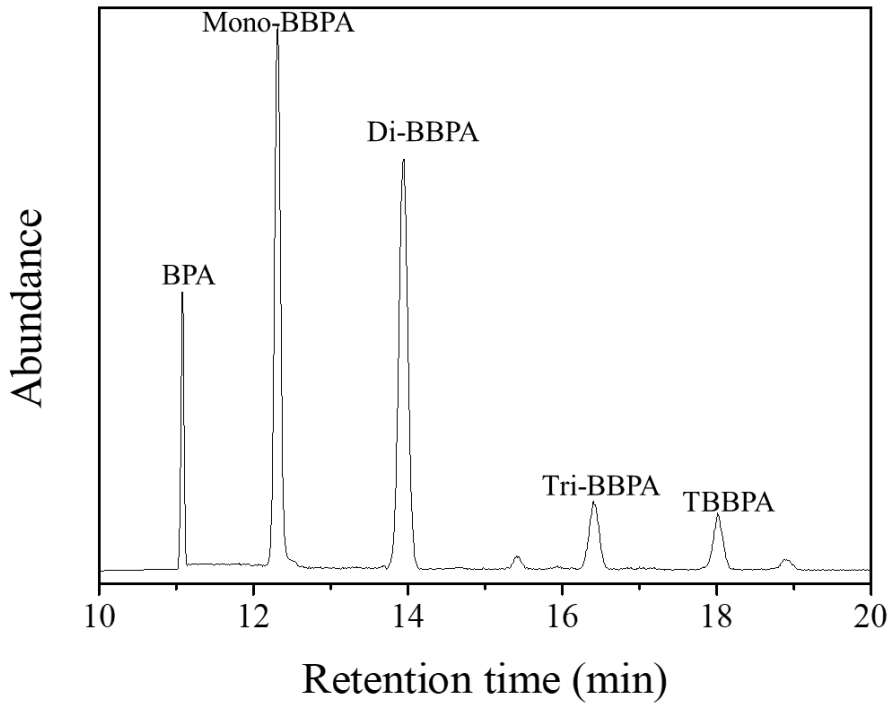

Figure S7. LC chromatogram for the TBBPA degradation and its transformation products in the S-nZVI system after anoxic treatment.

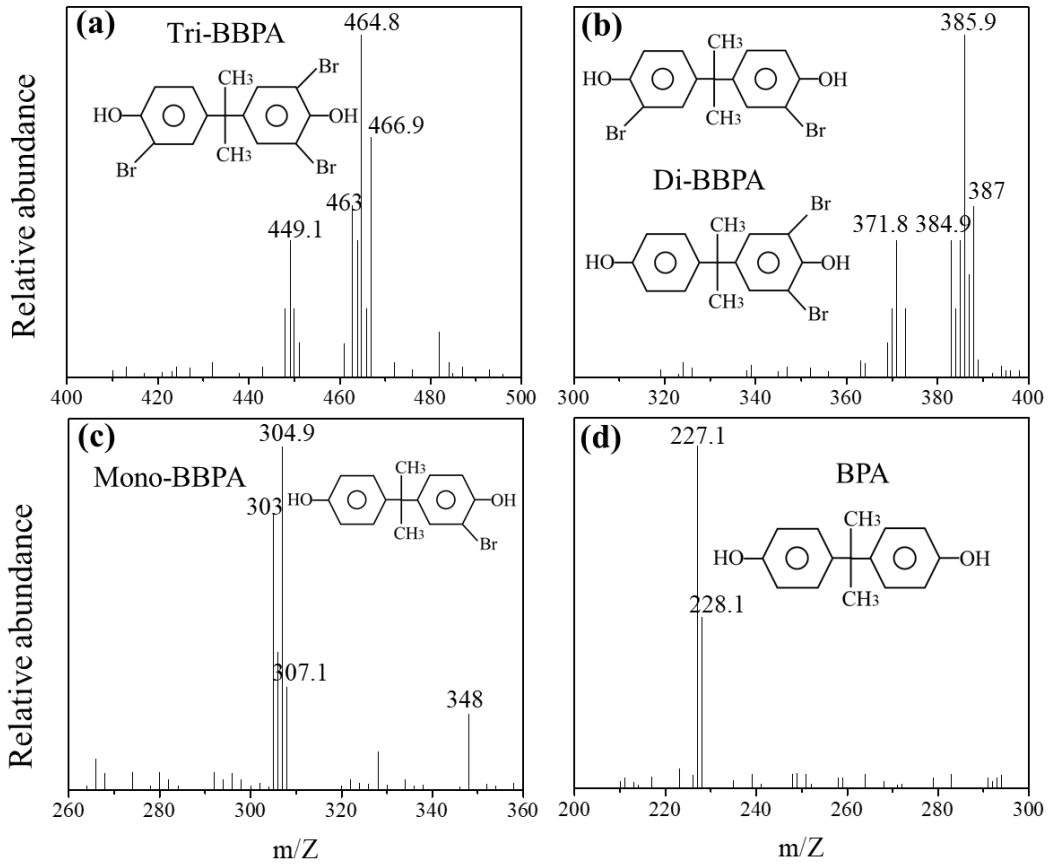

Figure S8. LC-MS spectra of the transformation products of TBBPA by S-nZVI under anoxic conditions. (a) Tri-BBPA; (b) Di-BBPA; (c) Mono-BBPA; (d) BPA.

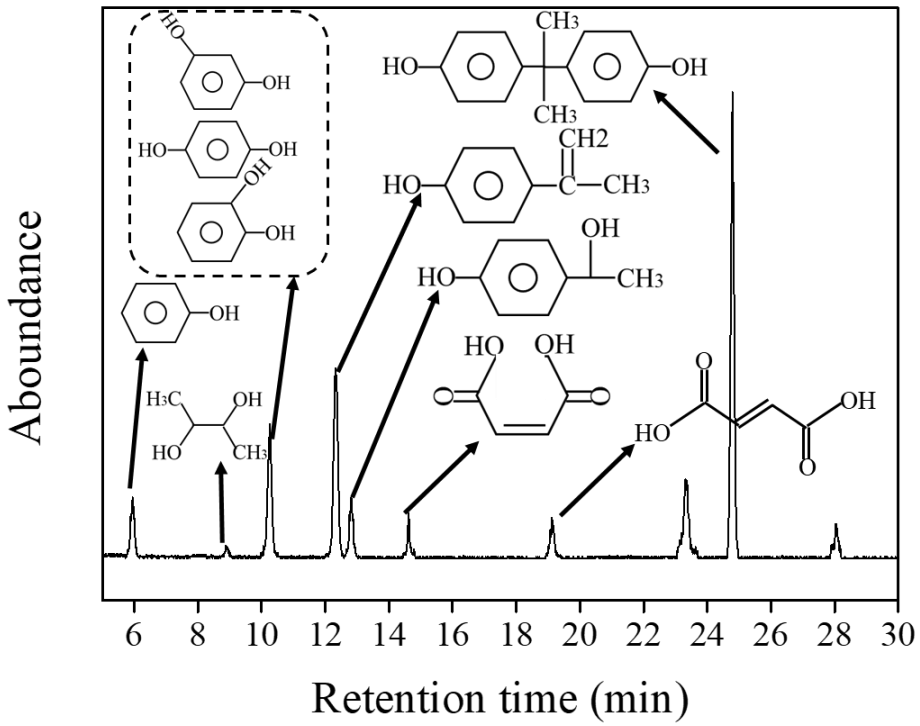

Figure S9. GC chromatogram for the BPA degradation and its transformation products in the S-nZVI system after oxic treatment.

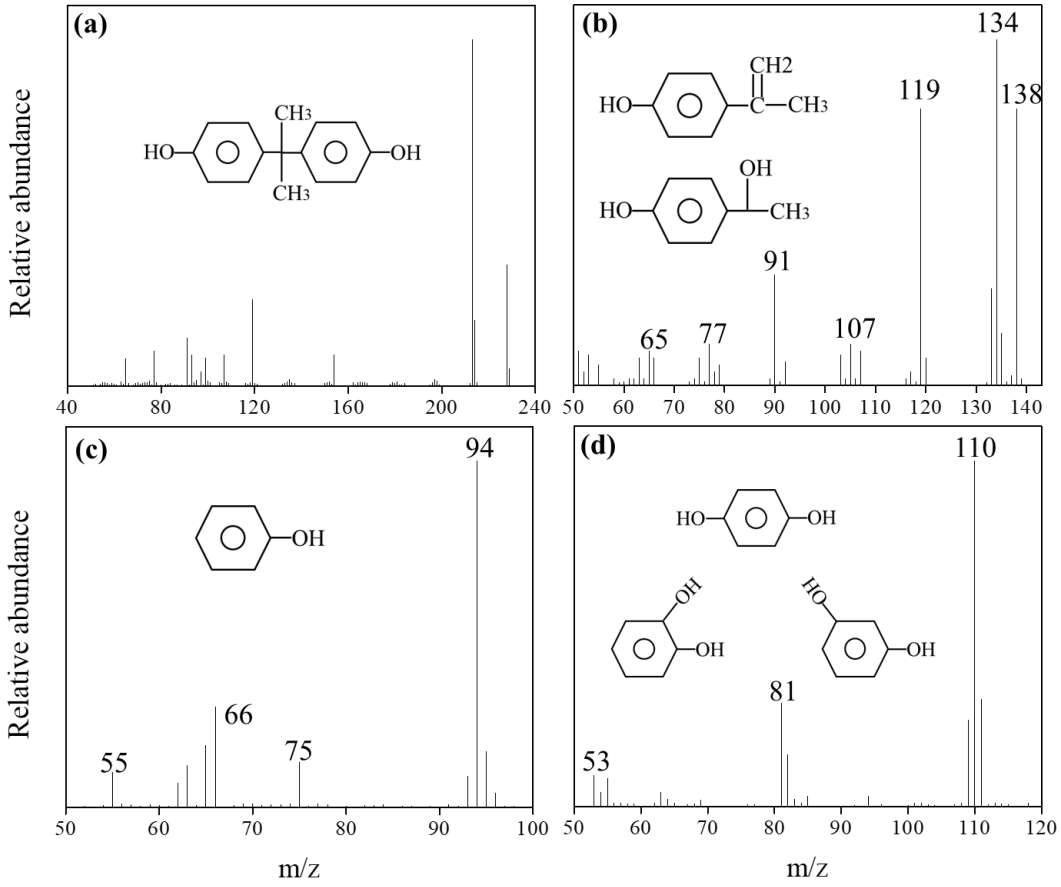

Figure S10. GC-MS spectra of the intermediates from BPA degradation by S-nZVI under oxic conditions.

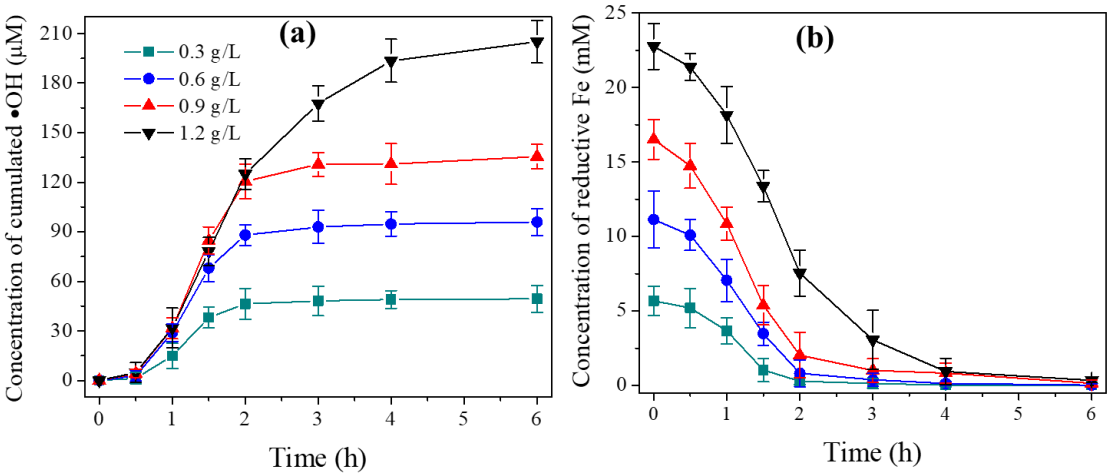

Figure S11. Concentrations of •OH and reductive Fe at different S-nZVI dosages under oxic conditions. (a) Cumulated concentrations of •OH and (b) total concentrations of reductive Fe (i.e., Fe(0) and Fe(II)) (legends for panel S11b follows the same symbolism as in S11a).

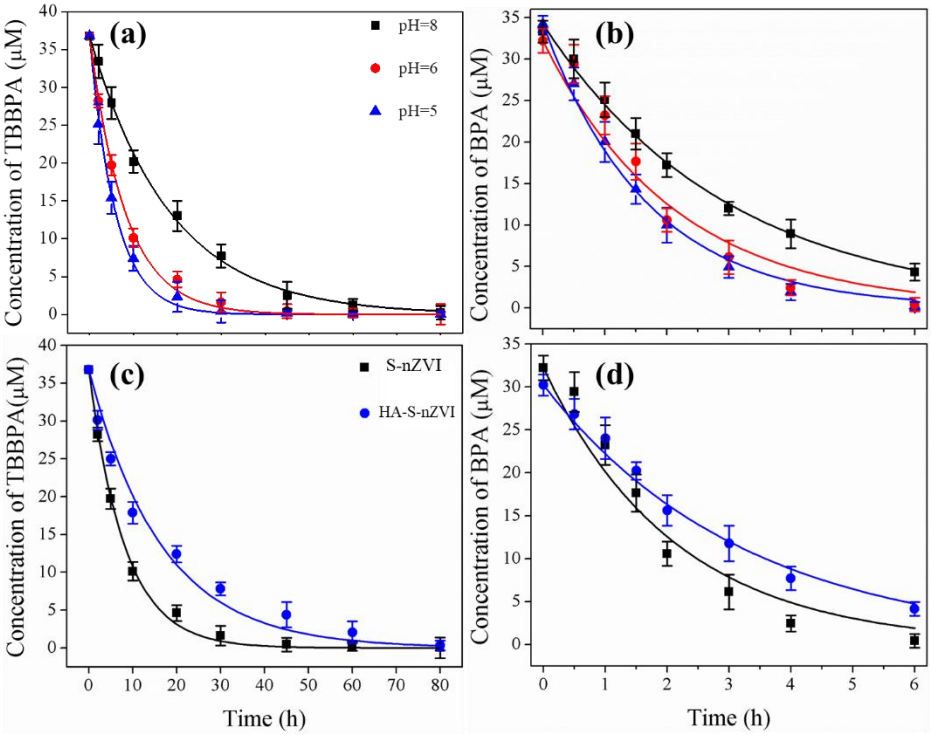

Figure S12. Effect of pH on (a) TBBPA degradation during anoxic stage and (b) BPA degradation under oxic condition. Experimental conditions: [S-nZVI] = 1.2 g/L. Effect of HA on (c) TBBPA degradation during anoxic stage and (d) BPA degradation during oxic stage. Experimental conditions: [S-nZVI] = 1.2 g/L, [HA] = 10 mg/L, initial pH = 6.0 ± 0.2 (legends for panel S12b follows the same symbols as in S12a, and S12d follows S12c, respectively).

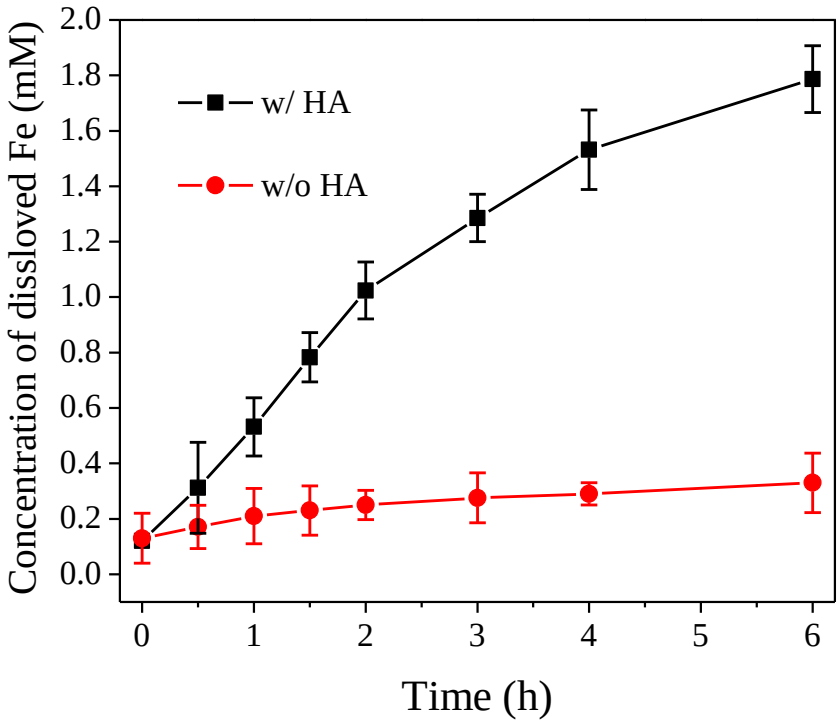

Figure S13. The release of soluble Fe from S-nZVI in the presence of HA under anoxic conditions. [S-nZVI] = 1.2 g/L, [HA] = 10 mg/L, initial pH = 6.0±0.2.

Table S1. The elemental compositions of HA.

C (%)[a,b]	H (%)	N (%)	O (%)[c]	Ash (%)
42.4 ± 5.6	4.9 ± 1.2	3.1 ± 0.7	50.8 ± 6.9	0.4 ± 0.06

[a] Mass-based percentages. [b]Errors given based on triplicate tests. [c]Calculated by mass balance.

Table S2. XPS results based on curve fitting for Fe $2p_{3/2}$ and S $2p_{3/2}$ peaks before and after the reaction shown in Figure S4.

Elements		B.E. (eV)[a]	Species	Relative fraction (%)	References
Fe ($2p_{3/2}$)	Fresh S-nZVI	707.3	Fe(II)-S	73.3	16, 17
		709.0	Fe(II)-O	10.4	18, 19
		709.3	Fe(III)-S	10.7	20
		710.6	Fe_3O_4	5.6	21
	After anoxic treatment	707.3	Fe(II)-S	54.5	16, 17
		709.0	Fe(II)-O	22.8	18, 19
		709.3	Fe(III)-S	15.4	20
		710.6	Fe_3O_4	7.3	21
	After oxic treatment	710.6	Fe_3O_4	4.6	21
		711.5	α-FeOOH/ Fe(III)-O	82.7	22 23
		713.0	Fe(III)-O	12.7	18
S ($2p_{3/2}$)	Fresh S-nZVI	161.3	S(-II)	46.6	20
		162.2	S_2(-II)	14.5	24
		163.4	S_n(-II)	30.8	18
		164.0	S_8	8.1	18
	After anoxic treatment	161.3	S(-II)	44.1	20
		162.2	S_2(-II)	15.8	24
		163.4	S_n(-II)	29.8	18
		164.0	S_8	10.3	18
	After oxic treatment	164.0	S_8	100	18

[a] B.E.=Binding Energy.

Table S3. Physical properties and surface area-normalized removal rates of S-nZVI as a function of different S/Fe molar ratio.

S/Fe molar ratios	Fe(0) content (wt %)[a]	S content (wt %)[b]	S_{BET} (m^2/g)[c]	$k_{SA} \times 10^{-4}$ (L m^{-2} h^{-1})[d]	R^2
0.1	84.6	3.9	23.5	6.63±0.25	0.992
0.2	83.5	6.0	27.5	27.8±1.06	0.996
0.3	83.1	7.9	33.6	30.5±0.97	0.997
0.5	83.0	9.0	32.4	9.52±0.40	0.993

[a]Fe(0) content was determined based on the H_2 production. [b]S content was quantified with carbon-sulfur analyzer. [c]The surface area was determined by N_2 adsorption using the Brunauer-Emmett-Teller (BET) method. [d]S_{BET}-normalized rate constant.

Table S4. Pseudo-first-order reaction rate model used for simulating TBBPA degradation kinetic data with different S-nZVI dosages during anoxic stage and the resulting fitting parameters (errors given as standard deviation).

S-nZVI dosage (g/L)	$k \times 10^{-2}$ (h^{-1})	R^2
0.3	2.06 ± 0.06	0.995
0.6	3.30 ± 0.14	0.992
0.9	6.15 ± 0.33	0.991
1.2	12.3 ± 0.39	0.997

Table S5. The pseudo-first-order rates of TBBPA, tri-BBPA, di-BBPA, and mono-BBPA by S-nZVI during anoxic stage and the resulting fitting parameters (errors given as standard deviation).

TBBPA transformation products	$k \times 10^{-2}$ (h^{-1})	R^2
TBBPA	12.3 ± 0.39	0.997
Tri-BBPA	9.57 ± 0.65	0.961
Di-BBPA	5.49 ± 0.37	0.940
Mono-BBPA	5.15 ± 0.16	0.980

Table S6. The effects of HA and pH on pseudo-first-order model fitted TBBPA and BPA degradation kinetics and the resulting fitting parameters (errors given as standard deviation).

Matters	HA[a]	pH	Conditions	$k \times 10^{-2}$ (h^{-1})	R^2
TBBPA	Y	6	Anoxic	6.03 ± 0.45	0.981
	N	6		12.3 ± 0.39	0.997
		5		17.0 ± 0.51	0.998
		8		5.47 ± 0.13	0.995
BPA	Y	6	Oxic	30.8 ± 1.36	0.988
	N	6		47.1 ± 4.72	0.958
		5		59.2 ± 2.29	0.991
		8		33.2 ± 0.80	0.994

[a] Y and N inidate with and without HA addition, respectively.

References

1. Eriksson, J.; Rahm, S.; Green, N.; Bergman, A.; Jakobsson, E., Photochemical transformations of tetrabromobisphenol A and related phenols in water. *Chemosphere* **2004,** *54*, (1), 117-126.

2. Wu, J.; Wang, X. B.; Zeng, R. J., Reactivity enhancement of iron sulfide nanoparticles stabilized by sodium alginate: Taking Cr (VI) removal as an example. *J. Hazard. Mater.* **2017,** *333*, 275-284.

3. Joo, S. H.; Feitz, A. J.; Sedlak, D. L.; Waite, T. D., Quantification of the oxidizing capacity of nanoparticulate zero-valent iron. *Environ. Sci. Technol.* **2005,** *39*, (5), 1263-1268.

4. Tong, M.; Yuan, S. H.; Ma, S. C.; Jin, M. G.; Liu, D.; Cheng, D.; Liu, X. X.; Gan, Y. Q.; Wang, Y. X., Production of abundant hydroxyl radicals from oxygenation of subsurface sediments. *Environ. Sci. Technol.* **2016,** *50*, (1), 214-221.

5. Katsoyiannis, I. A.; Ruettimann, T.; Hug, S. J., pH dependence of Fenton reagent generation and As(III) oxidation and removal by corrosion of zero valent iron in aerated water. *Environ. Sci. Technol.* **2008,** *42*, (19), 7424-7430.

6. Wu, J.; Zeng, R. J., In situ preparation of stabilized iron sulfide nanoparticle-impregnated alginate composite for selenite remediation. *Environ. Sci. Technol.* **2018,** *52*, (11), 6487-6496.

7. Jeong, H. Y.; Han, Y. S.; Park, S. W.; Hayes, K. F., Aerobic oxidation of mackinawite (FeS) and its environmental implication for arsenic mobilization. *Geochim. Cosmochim. Ac.* **2010,** *74*, (11), 3182-3198.

8. Han, Y. L.; Yan, W. L., Reductive dechlorination of trichloroethene by zero-valent iron nanoparticles: Reactivity enhancement through sulfidation treatment. *Environ. Sci. Technol.* **2016,** *50*, (23), 12992-13001.

9. Cao, Z.; Liu, X.; Xu, J.; Zhang, J.; Yang, Y.; Zhou, J. L.; Xu, X. H.; Lowry, G. V., Removal of antibiotic florfenicol by sulfide-modified nanoscale zero-valent iron. *Environ. Sci. Technol.* **2017,** *51*, (19), 11269-11277.

10. He, F.; Li, Z.; Shi, S.; Xu, W.; Sheng, H.; Gu, Y.; Jiang, Y.; Xi, B., Dechlorination

of excess trichloroethene by bimetallic and sulfidated nanoscale zero-valent iron. *Environ. Sci. Technol.* **2018**.

11. Chirita, P.; Descostes, M.; Schlegel, M. L., Oxidation of FeS by oxygen-bearing acidic solutions. *J. Colloid Interf. Sci.* **2008,** *321*, (1), 84-95.

12. Liu, T. Z.; Tsang, D. C. W.; Lo, I. M. C., Chromium(VI) reduction kinetics by zero-valent iron in moderately hard water with humic acid: Iron dissolution and humic acid adsorption. *Environ. Sci. Technol.* **2008,** *42*, (6), 2092-2098.

13. Hicks, M.; Gebicki, J. M., Rate constants for reaction of hydroxyl radicals with tris, tricine and hepes buffers. *Febs Lett.* **1986,** *199*, (1), 92-94.

14. Tan, L.; Liang, B.; Fang, Z. Q.; Xie, Y. Y.; Tsang, E. P., Effect of humic acid and transition metal ions on the debromination of decabromodiphenyl by nano zero-valent iron: kinetics and mechanisms. *J. Nanopart. Res.* **2014,** *16*, (12).

15. Tratnyek, P. G.; Scherer, M. M.; Deng, B. L.; Hu, S. D., Effects of natural organic matter, anthropogenic surfactants, and model quinones on the reduction of contaminants by zero-valent iron. *Water Res.* **2001,** *35*, (18), 4435-4443.

16. Herbert, R. B.; Benner, S. G.; Pratt, A. R.; Blowes, D. W., Surface chemistry and morphology of poorly crystalline iron sulfides precipitated in media containing sulfate-reducing bacteria. *Chemical Geology* **1998,** *144*, (1-2), 87-97.

17. Behra, P.; Bonnissel-Gissinger, P.; Alnot, M.; Revel, R.; Ehrhardt, J. J., XPS and XAS study of the sorption of Hg(II) onto pyrite. *Langmuir : the ACS journal of surfaces and colloids* **2001,** *17*, (13), 3970-3979.

18. Thomas, J. E.; Jones, C. F.; Skinner, W. M.; Smart, R. S., The role of surface sulfur species in the inhibition of pyrrhotite dissolution in acid conditions. *Geochim. Cosmochim. Ac.* **1998,** *62*, (9), 1555-1565.

19. Yamashita, T.; Hayes, P., Analysis of XPS spectra of Fe^{2+} and Fe^{3+} ions in oxide materials. *Appl. Surf. Sci.* **2008,** *254*, (8), 2441-2449.

20. Pratt, A. R.; Nesbitt, H. W.; Muir, I. J., Generation of acids from mine waste-oxidative leaching of pyrrhotite in dilute H_2SO_4 solutions at pH 3.0. *Geochim. Cosmochim Ac.* **1994,** *58*, (23), 5147-5159.

21. Carver, J. C.; Carlson, T. A.; Schweitzer, G. K., Use of X-ray photoelectron

spectroscopy to study bonding in Cr, Mn, Fe, and Co compounds. *J. Chem. Phys.* **1972,** *57*, (2), 973-982.

22. Konno, H.; Nagayama, M., X-ray photoelectron-spectra of hexavalent iron. *J. Electron. Spectrosc.* **1980,** *18*, (4), 341-343.

23. Mcintyre, N. S.; Zetaruk, D. G., X-ray photoelectron spectroscopic studies of iron-oxides. *Anal. Chem.* **1977,** *49*, (11), 1521-1529.

24. Li, D.; Zhu, X. F.; Zhong, Y.; Huang, W. L.; Peng, P., Abiotic transformation of hexabromocyclododecane by sulfidated nanoscale zerovalent iron: Kinetics, mechanism and influencing factors. *Water Res.* **2017,** *121*, 140-149.